47th AIAA/ASME/SAE/ASEE Joint Propulsion Conference & Exhibit
31 July - 03 August 2011, San Diego, California

AIAA 2011-5648

Biglobal Instability of the Bidirectional Vortex. Part 1: Formulation

Joshua W. Batterson* and Joseph Majdalani†
University of Tennessee Space Institute, Tullahoma, TN 37388, USA

Hydrodynamic instability research has begun to shift from the one-dimensional analysis of the Orr-Sommerfeld, local nonparallel, and parabolic type to the two-dimensional, biglobal analysis. Classic methods, such as the local nonparallel approach, specify a one-dimensional amplitude function *a priori* so that streamwise and azimuthal variations become characterized by a complex wave and integer mode number, respectively. This formulation is heavily dependent on the so-called *parallel flow assumption*. In brief, this property requires the streamlines of the baseflow to be parallel or nearly parallel, a condition that may be quite restrictive at times. It can therefore be seen that the use of biglobal analysis becomes necessary to encompass a broader range of baseflows. The relatively novel, two-dimensional characterization of the hydrodynamic waveform gives rise to a more complete analysis that intrinsically captures spatial instability behavior while remaining unrestricted to special geometries, such as elongated rocket chambers. The biglobal approach only requires periodicity in the tangential direction and seems to be tailor-made for cylindrical axisymmetric flows, such as those arising in the bidirectional vortex engine. Moreover, for short rocket chambers such as those associated with bidirectional vortex engines, the parallel flow assumption cannot be justified, and one finds the biglobal analysis as a more suitable alternative to the local nonparallel (LNP) approach used extensively in solid rocket motor stability investigations. However, being multi-dimensional, the biglobal technique requires more effort than its predecessor, specifically in the analytical derivation, numerical discretization, and spectral collocation tools necessitated by the treatment of the resulting partial differential equations. The present work serves to offer a detailed description of the theoretical framework and numerical tools needed to tackle this problem in the context of a confined vortex chamber such as that investigated by NASA/ORBITEC.

Nomenclature

A_{ij}	=	the operator matrix
B_{ij}	=	the right-hand-side coefficient matrix of a matrix pencil
D_N	=	the Chebyshev pseudo-spectral derivative matrix of size N
d	=	weight coefficients for pseudo-spectral derivative matrices
I_N	=	the identity matrix of size N
l	=	chamber aspect ratio
M	=	baseflow component
$\tilde{M}$	=	instantaneous flow component
m	=	general amplitude function
$\hat{m}$	=	acoustic fluctuation
$\check{m}$	=	hydrodynamic fluctuation
m'	=	general fluctuation
$\tilde{m}$	=	vortical fluctuation
P	=	baseflow pressure
$\tilde{P}$	=	instantaneous pressure
p	=	pressure amplitude function
$\check{p}$	=	hydrodynamic pressure fluctuation
$\hat{p}$	=	acoustic pressure fluctuation
p'	=	general pressure fluctuation
$\tilde{p}$	=	vortical pressure fluctuation
q	=	azimuthal integer wave number
r	=	radial nondimensional coordinate
Re	=	Reynolds number, Ua/ν

*Graduate Research Assistant, Mechanical, Aerospace and Biomedical Engineering Department. Student Member AIAA.
†H. H. Arnold Chair of Excellence in Advanced Propulsion and Professor, Mechanical, Aerospace and Biomedical Engineering Department Associate Fellow AIAA. Fellow ASME.

T_N = Chebyshev polynomial of the first kind
$\boldsymbol{U}$ = baseflow velocity vector, $U_r\boldsymbol{e}_r + U_\theta\boldsymbol{e}_\theta + U_z\boldsymbol{e}_z$
$\tilde{U}$ = instantaneous flow velocity
U = average tangential inlet velocity (dimensional)
u = velocity amplitude function
$\check{u}$ = hydrodynamic velocity fluctuation
$\hat{u}$ = acoustic velocity fluctuation
u' = general velocity fluctuation
$\tilde{u}$ = vortical velocity fluctuation
V = vortex Reynolds number, $V = 2\pi\kappa/\varepsilon$
z = nondimensional axial coordinate

Greek
α = longitudinal wave number
β = normalized outlet radius, b/a
∇ = gradient operator
δ = characteristic boundary layer thickness
ε = $1/Re$
η = streamwise Chebyshev variables mapped between $[-1, 1]$
κ = inflow parameter, $(2\pi\sigma l)^{-1}$
λ = eigenvalue
ω = frequency of oscillation, $\omega_r + \omega_i$
σ = swirl number
θ = nondimensional tangential coordinate
ν = kinematic viscosity
ξ = radial Chebyshev variables mapped between $[-1, 1]$

Subscripts
ii = denotes a diagonal matrix or diagonal element
ij = denotes a matrix
N = Chebyshev polynomial order/number of collocation points

Superscripts
n = denotes the order of the derivative
$\bar{}$ = denotes dimensional variables

Abbreviations
DNS = direct numerical simulation
LNP = local nonparallel
LNS = linearized Navier-Stokes
NPR = nonparallel ratio
ODE = ordinary differential equation
PDE = partial differential equation
VCCWC = Vortex Combustion Cold-Wall Chamber

I. Introduction

This study seeks to engage two separate, yet equally interesting topics of research: the bidirectional vortex flowfield and biglobal instability. Both topics are common conversational pieces in rocket propulsion as well as in general fluid dynamics. Although neither the topic of general vortex flows nor hydrodynamic instabilities are entirely new, modern developments in each have led to the opportunity of better understanding the transition to turbulence in the Vortex Combustion Cold-Wall Chamber (VCCWC) developed by Chiaverini, Knuth and co-workers. [1–3] This engine configuration is depicted in Fig. 1 where its main flow properties are displayed. In what follows, both concepts will be briefly introduced.

From a broader perspective, swirling flows are of fundamental importance to a number of fields. The strategic development of vortices in industrial devices such as cyclonic furnaces have been shown to promote increased combustion efficiency by increasing combustion residence time as well as presenting a flow regime that is more conducive to mixing. Vortex flows are of meteorological interest when considering geophysical phenomena such as tornadoes, hurricanes, water spouts, and dust devils. A comprehensive review of analytical models describing such phenomena has been compiled in the first half of the paper by Batterson and Majdalani. [4] Classic work on unidirectional vortex flows has produced models named after Rankine, [5] Lamb-Oseen, [6] and Burgers-Rott. [7] Vatistas and coworkers [8,9] have also contributed toward analytical, numerical, and experimental understanding of vortex flows. Their recent endeavors have broached the topic of compressibility in vortices. [10]

Bidirectional swirl-driven flowfield models include a solution by Sullivan [11] who produced an analytical profile for bidirectional external vortices. More recently, Bloor and Ingham [12,13] studied the internal bidirectional flowfield of cyclonic separators. Devices of this type are found in the mineral, chemical, and filtration industries. Corresponding technologies are directly pertinent to the refinement of uranium for nuclear power generation and weaponry. In the context of liquid rocket propulsion, the reader is referred to a set of articles on the Vortex Combustion Cold-Wall Chamber under development by ORBITEC (e.g. Chiaverini *et al.* [1–3]). Analytical models that support the VCCWC concept have been under investigation since 2003 when an exact inviscid solution was presented by Vyas, Majdalani and Chiaverini, [14] and later refined by Vyas and Majdalani. [15] Although their analysis was constructed under non-reacting, cold-flow conditions, it laid the groundwork for modeling swirl-driven liquid rocket engines. The problem was revisited by Majdalani and Chiaverini [16] who suggested viscous corrections to remove the unphysical tangential core singularity common to inviscid vortex motions. They continued further by applying a similar technique to satisfy the no-slip condition at the wall in the tangential direction. Along similar lines, Batterson and Majdalani [17] developed viscous boundary layer corrections for the remaining axial and radial components. Majdalani [18] went further to develop two inviscid bidirectional vortex models of the Beltramian type using the Bragg-Hawthorne equation as a starting point. These too required the application of boundary layer theory, a task that was quickly carried out by Batterson and Majdalani; [19,20] the latter also explored the possibility of multidirectional vortex motions. [21]

Concerning the instability of the bidirectional vortex, the first related study was performed by Abu-Irshaid, Majdalani and Casalis. [22] As we expand beyond their one-dimensional, local nonparallel formulation, we reexamine the problem of hydrodynamic instability in the bidirectional vortex using a biglobal approach. The shift from a one to a two-dimensional hydrodynamic stability framework stands to improve our understanding of laminar to turbulent flow transition. Both one-dimensional and biglobal models decompose the flow into a leading-order mean flow and a higher-order, small-amplitude disturbance. [23] The effect of the disturbance on the overall flowfield is subsequently explored through various analytical, numerical, and experimental techniques. One-dimensional instability models are helpful when considering parallel flows in which the Navier-Stokes equations only contain an essentially one-dimensional gradient. Although such problems provide insight into the general behavior, they are limited to rudimentary flows. Biglobal instability techniques allow for less-idealized, multi-dimensional motions to be readily handled. This is especially true in view of modern computational tools that have greatly facilitated the task of resolving the difficult sub-problems associated with the biglobal method.

Given the recent growth in flowfield instability research, biglobal approaches have become a topic of keen interest to many investigators. By way of example, insights into the stability of rectangular ducts and cavities have been presented by Theofilis, Duck and Owen. [24] In the same vein, duct flow stability of constricted motions has been advanced by Pitt, Sherwin and Theofilis. [25] Chedevergne and Casalis, [26] and Chedevergne, Casalis and Féraille [27] have studied the effect of small perturbations on the classic Taylor-Culick profile in solid rocket motors. Chedevergne, Casalis and Majdalani [28] have also showed that DNS calculations could reproduce hydrodynamic instability waves when augmented by vortico-acoustic contributions. Because of the similarity between the Taylor-Culick and the bidirectional vortex models, these two studies will be at the forefront of the present analysis. In what follows, the general biglobal instability framework will be methodically developed with a presentation of the analytical formulation of the cylindrical equations, spectral decomposition, and the fundamentals of iterative eigensolvers.

A. Nondimensionalization

The sinusoidal, complex-lamellar solution of the bidirectional vortex is presented in work by Vyas and Majdalani. [15] Our paper follows by considering the same case of a cylindrical tube of length L and radius a with a closed headwall and an exit port at the aft end whose dimensional radius is denoted by b. We also assume that purely tangential injectors are located at the base to induce swirl. This geometry is best visualized in Fig. 1b. The

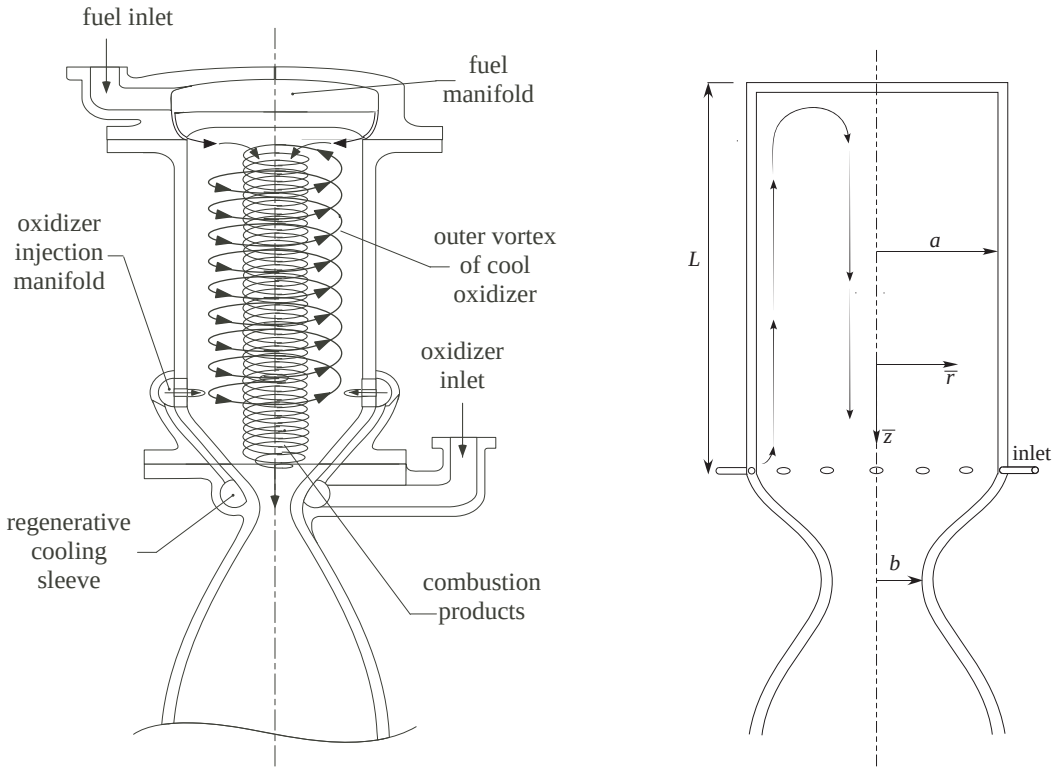

a) VCCWC schematic **b)** VCCWC geometry

Figure 1. VCCWC schematic and geometry.

axial velocity at the injectors is deemed small in comparison to the tangential component and thus negligible in the mathematical model. Additionally, the distribution of tangential injection at the base is assumed to be uniform, as one may associate with a circular line source. This allows for the assumption of axisymmetry at the onset of injection where, in a real three-dimensional fluid, it could only be realized after the flow has traversed a finite distance away from the aft end. Subsequently, the governing equations are devised under the conditions of:

1. Steady* (mean flow only)
2. Inviscid* (mean flow only)
3. Axisymmetric* (mean flow only)
4. Incompressible
5. Rotational
6. Nonreactive/cold-flow
7. Axially independent swirl velocity* (mean flow only)

* Assumptions restricting the mean flow only. Not included in the stability formulation.

It is helpful to nondimensionalize all lengths by the radius and all velocities by the characteristic velocity (the tangential injection velocity U). Other normalizations are devised on the basis of convenience or to eliminate extraneous dimensional constants. Our convention comprises:

$$\begin{cases} z = \dfrac{\bar{z}}{a}; \quad r = \dfrac{\bar{r}}{a}; \quad t = \bar{t}\dfrac{U}{a}; \quad l = \dfrac{L}{a}; \quad \nabla = a\bar{\nabla}; \quad Re = \dfrac{Ua}{\nu}; \\ \tilde{U}_r = \dfrac{\bar{U}_r}{U}; \quad \tilde{U}_\theta = \dfrac{\bar{U}_\theta}{U}; \quad \tilde{U}_z = \dfrac{\bar{U}_z}{U}; \quad \tilde{P} = \dfrac{\bar{P}}{\rho U^2}; \quad Q_i = \dfrac{\bar{Q}_i}{Ua^2}; \end{cases} \tag{1}$$

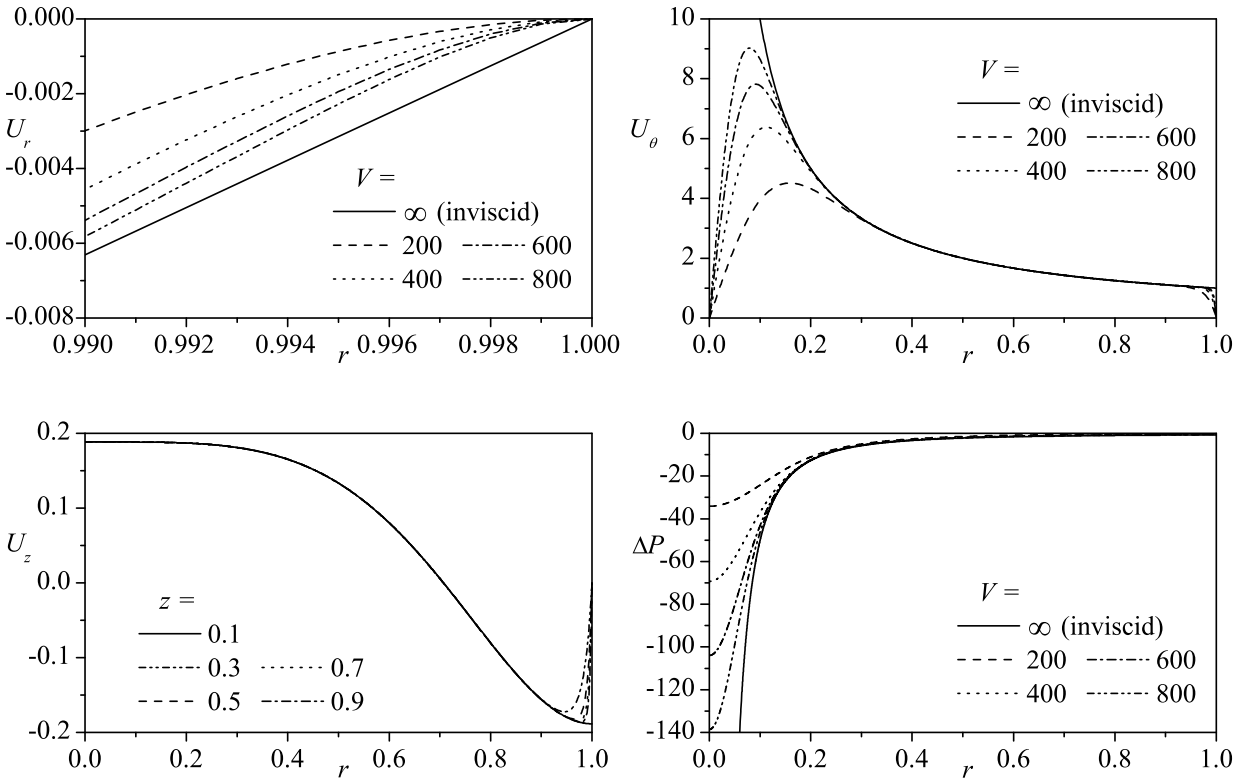

Figure 2. The viscous, complex-lamellar, bidirectional vortex with $\kappa = 0.103$ and $z = 0.3$.

II. Bidirectional Vortex Models

For the sake of brevity, we refer the reader to the papers by Vyas and Majdalani, [15] Majdalani and Chiaverini, [16] and those by Batterson and Majdalani [17,19–21] for the comprehensive characterization of the various bidirectional vortex models. In short, we find the uniformly valid, *ad hoc* velocity and pressure solutions for each flowfield to be:

Complex-Lamellar Model (Fig. 2):

$$U_r(r) = -\kappa r^{-1}\sin\left(\pi r^2\right)\left[1 - e^{-\frac{V}{4}\alpha\left(1-r^2\right)}\right] \tag{2}$$

$$U_\theta = r^{-1}\left[1 - e^{-\frac{V}{4}r^2} - e^{-\frac{V}{4}\alpha\left(1-r^2\right)}\right]; \tag{3}$$

$$U_z(r,z) = 2\pi\kappa z\cos\left(\pi r^2\right)\left[1 - e^{-\frac{V}{4}\alpha\left(1-r^2\right)}\right] \tag{4}$$

$$\begin{aligned}\Delta P = -\frac{1}{2r^2}\left\{\left(1 - e^{-\frac{1}{4}Vr^2}\right)^2 + \left[1 - e^{-\frac{1}{4}\alpha V\left(1-r^2\right)}\right]^2 - 1 + 2e^{\frac{1}{4}V\left[\alpha+(1-\alpha)r^2\right]}\right\}\\ -\frac{1}{4}V\left\{\mathrm{Ei}\left(-\tfrac{1}{2}Vr^2\right) - \mathrm{Ei}\left(-\tfrac{1}{4}Vr^2\right) + \alpha e^{-\frac{1}{4}\alpha V}\left[\mathrm{Ei}\left(\tfrac{1}{4}\alpha Vr^2\right) - \mathrm{Ei}\left(\tfrac{1}{4}\alpha V\right)\right]\right.\\ \left. -\alpha e^{-\frac{1}{2}\alpha V}\left[\mathrm{Ei}\left(\tfrac{1}{2}\alpha Vr^2\right) - \mathrm{Ei}\left(\tfrac{1}{2}\alpha V\right)\right]\right\}\end{aligned} \tag{5}$$

Linear Beltramian Model (depicted in Fig. 3):

$$U_r = -\frac{\kappa J_1(\lambda_0 r)}{\beta J_1(\lambda_0\beta)}\left\{1 - \exp\left[-\frac{\lambda_0 V}{4\pi\beta J_1(\lambda_0\beta)}\left(\frac{\lambda_0^2}{8} - 1\right)(1-r)\right]\right\} \tag{6}$$

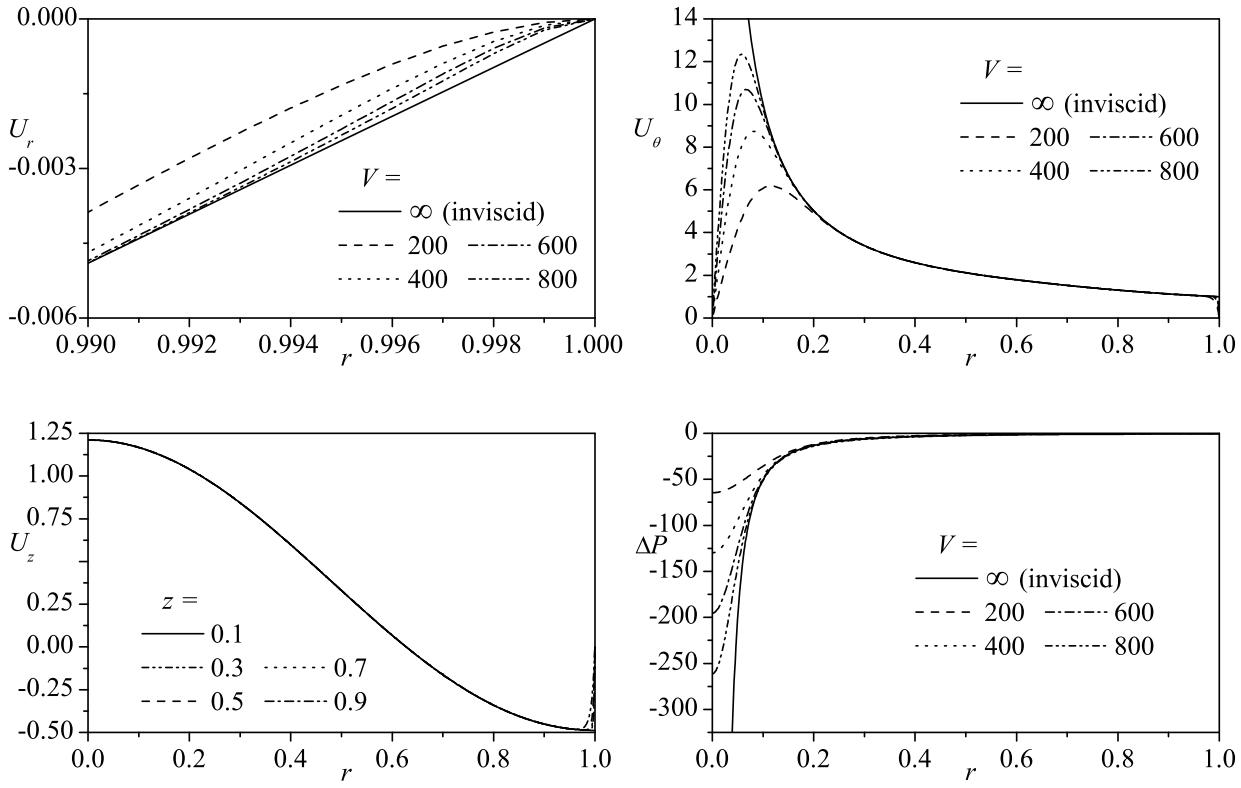

Figure 3. The viscous, linear Beltramian, bidirectional vortex with $\kappa = 0.103$ and $z = 1$.

$$U_\theta = \frac{1}{r}\left\{\left[1 + \frac{\lambda_0^2\kappa^2 r^2 z^2 J_1^2(\lambda_0 r)}{\beta^2 J_1^2(\lambda_0\beta)}\right]^{1/2} - \exp\left[-\frac{\lambda_0 V r^2}{8\pi\beta J_1(\lambda_0\beta)}\right] - \exp\left[-\frac{\lambda_0 V}{4\pi\beta J_1(\lambda_0\beta)}\left(\frac{\lambda_0^2}{8} - 1\right)(1-r)\right]\right\} \tag{7}$$

$$U_z = \frac{\lambda_0\kappa z J_0(\lambda_0 r)}{\beta J_1(\lambda_0\beta)}\left\{1 - \exp\left[-\frac{\lambda_0 V}{4\pi\beta J_1(\lambda_0\beta)}\left(\frac{\lambda_0^2}{8} - 1\right)(1-r)\right]\right\} \tag{8}$$

$$\begin{aligned}\Delta P(r,z) = {} & \frac{r^2-1}{2r^2} + \frac{1}{2}e^{-\frac{V}{\pi}\gamma} - e^{-\frac{V}{2\pi}\gamma} + \frac{1}{r^2}\left(e^{-\frac{V}{2\pi}\gamma r^2} - \frac{1}{2}e^{-\frac{V}{\pi}\gamma r^2}\right) \\ & + \frac{V}{2\pi}\gamma\left[\mathrm{Ei}\left(-\frac{V}{\pi}\gamma\right) - \mathrm{Ei}\left(-\frac{V}{\pi}\gamma r^2\right) + \mathrm{Ei}\left(-\frac{V}{2\pi}\gamma r^2\right) - \mathrm{Ei}\left(-\frac{V}{2\pi}\gamma\right)\right] \\ & + \frac{1}{2} + \frac{V}{2\pi}\alpha - \frac{V^2}{2\pi^2}\alpha^2\mathrm{Ei}\left(\frac{V}{\pi}\alpha\right)e^{-\frac{V}{\pi}\alpha} + \frac{1}{2r^2\varepsilon^2}\left(-e^{-\frac{V}{\pi}\alpha(1-r)}\varepsilon(\varepsilon + 2r\alpha\kappa) + 4r^2\alpha^2\kappa^2 e^{-\frac{V}{\pi}\alpha}\mathrm{Ei}\left(\frac{V}{\pi}\alpha r\right)\right) \\ & - \frac{4\pi^2\kappa^2 + 2\pi\alpha V\kappa^2 - \alpha^2\kappa^2\mathrm{Ei}\left(\frac{V}{2\pi}\alpha\right)e^{-\frac{V}{2\pi}\alpha}}{4\pi^2\kappa^2} + \frac{\left(4\pi^2\kappa^2 + 2\pi V\kappa^2\alpha r\right)e^{-\frac{V}{2\pi}\alpha(1-r)} - r^2V^2\alpha^2\kappa^2 e^{-\frac{V}{2\pi}\alpha}\mathrm{Ei}\left(\frac{V}{2\pi}\alpha r\right)}{4\pi^2\kappa^2 r^2} \\ & + \frac{z^2\kappa^2\lambda_0^2}{2\beta^2 J_1(\lambda_0\beta)}\left[J_0^2(\lambda_0) - J_0^2(\lambda_0 r) + J_1^2(\lambda_0) - J_1^2(\lambda_0 r)\right]\end{aligned} \tag{9}$$

Harmonic Beltramian Model (depicted in Fig. 4):

$$U_r = -\frac{\pi\kappa}{2\beta J_1(\lambda_0\beta)}\cos\left(\tfrac{1}{2}\pi z/l\right)J_1(\lambda_0 r)\left\{1 - \exp\left[-\frac{V}{2\pi}\alpha(1-r)\right]\right\} \tag{10}$$

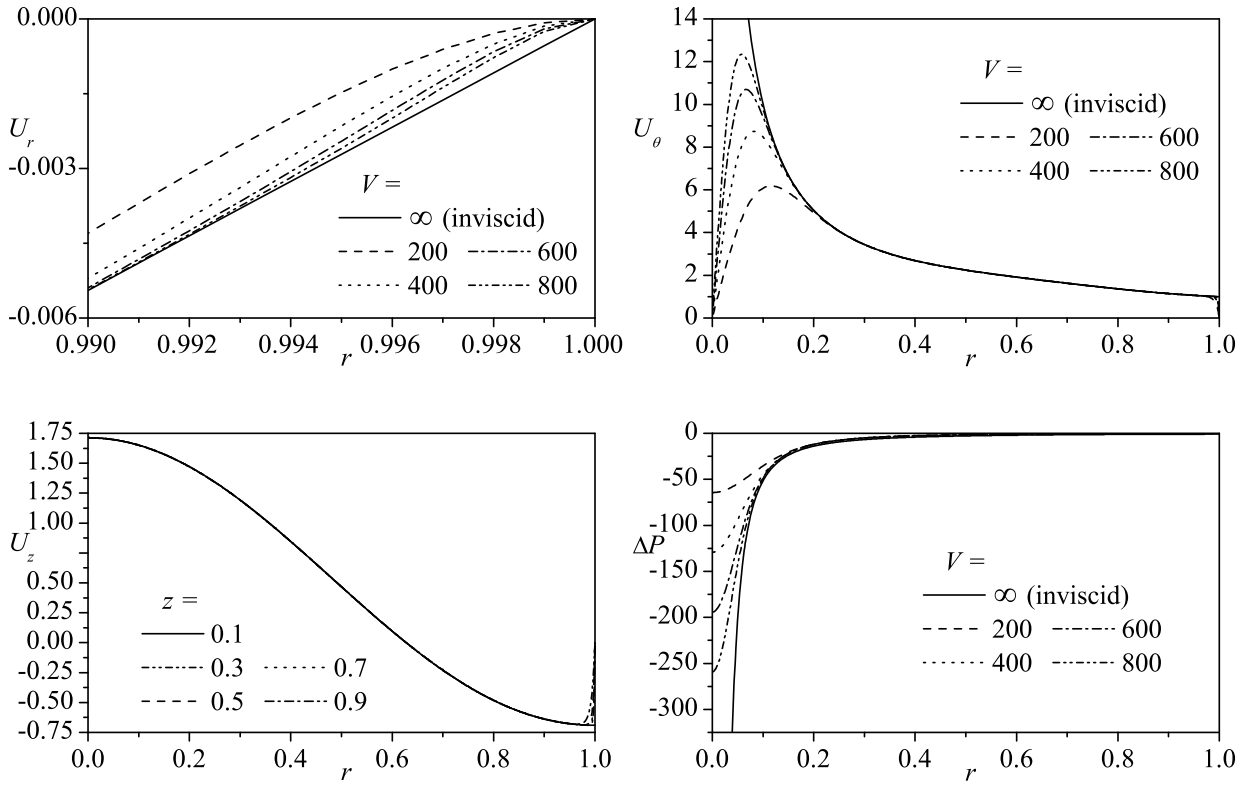

Figure 4. The viscous, harmonic Beltramian, bidirectional vortex with $\kappa = 0.103$, $l = 2$, and $z = 1$.

$$U_\theta = r^{-1}\left\{\left[1+\frac{\kappa^2}{\beta^2 J_1^2(\lambda_0\beta)}\left(\lambda_0^2 l^2+\frac{1}{4}\pi^2\right)r^2\sin^2\left(\tfrac{1}{2}\pi z/l\right)J_1^2(\lambda_0 r)\right]^{1/2} - \exp\left(-\frac{V}{2\pi}\gamma r^2\right) - \exp\left[-\frac{V}{2\pi}\alpha(1-r)\right]\right\} \tag{11}$$

$$U_z = \frac{\lambda_0\kappa l}{\beta J_1(\lambda_0\beta)}\sin\left(\tfrac{1}{2}\pi z/l\right)J_0(\lambda_0 r)\left\{1-\exp\left[-\frac{V}{2\pi}\alpha(1-r)\right]\right\} \tag{12}$$

$$\begin{aligned}\Delta P(r,z) = {} & \frac{r^2-1}{2r^2} - \frac{V}{2\pi}\alpha + \frac{\pi^2+\pi\alpha V-\alpha^2V^2\mathrm{Ei}\left(\frac{V}{\pi}\alpha\right)e^{-\frac{V}{\pi}\alpha}}{2\pi^2} \\ & - \frac{\pi(\pi+V\alpha r)e^{-\frac{V}{\pi}\alpha(1-r)} - r^2\alpha^2V^2\mathrm{Ei}\left(\frac{V}{\pi}\alpha r\right)e^{-\frac{V}{\pi}\alpha}}{2\pi^2r^2} \\ & + \frac{1}{r^2}\left(e^{-\frac{V}{2\pi}\gamma r^2} - \frac{1}{2}e^{-\frac{V}{\pi}\gamma r^2}\right) + \frac{\pi}{2\pi}\left(e^{-\frac{V}{\pi}\gamma} - 2e^{-\frac{V}{2\pi}\gamma}\right) + \frac{V\gamma}{2\pi}\left[\mathrm{Ei}\left(-\frac{V}{\pi}\gamma\right) - \mathrm{Ei}\left(-\frac{V}{\pi}\gamma r^2\right)\right] \\ & + \frac{V\gamma}{2\pi}\left[\mathrm{Ei}\left(-\frac{V}{2\pi}\gamma r^2\right) - \mathrm{Ei}\left(-\frac{V}{2\pi}\gamma\right)\right] + \frac{\alpha^2V^2}{4\pi^2}\mathrm{Ei}\left(\frac{V}{2\pi}\alpha\right)e^{-\frac{V}{2\pi}\alpha} \\ & + \frac{2\pi(2\pi+V\alpha r)e^{-\frac{V}{2\pi}\alpha(1-r)} - r^2\alpha^2V^2\mathrm{Ei}\left(\frac{V}{2\pi}\alpha r\right)e^{-\frac{V}{2\pi}\alpha}}{4r^2\pi^2}\end{aligned} \tag{13}$$

III. On Linear Hydrodynamic Stability Theory

To initiate the stability characterization, the instantaneous velocity is decomposed into the sum of a steady part [‡] and three oscillating perturbations,

$$\tilde{M} = M + \hat{m} + \tilde{m} + \check{m} \tag{14}$$

Here $\tilde{M}$ represents the instantaneous flow component and M denotes the baseflow. Next, the compressible, irrotational acoustic wave, $\hat{m}$, combines with the rotational, incompressible vortical wave, $\tilde{m}$, to form the vortico-acoustic wave. [29] These two are coupled through the no-slip condition at the wall. The frequencies of these waves are computed from the zeros of a sinusoidal, linear wave and correspond to the natural frequencies of the chamber. The hydrodynamic wave is given as $\check{m}$. It is generally described as a *parietal* instability that is spawned from flow interactions with sidewall boundaries. While it is common that the highest amplitude oscillations occur near the wall, it is not always the case. Hydrodynamic breakdown can take place over the entire volume and is likely to manifest itself wherever rotationality is present. Unlike the vortico-acoustic wave, it occurs over a wide spectrum of frequencies and scales that are characteristic of turbulence. Furthermore, it independently satisfies both acoustic and no-slip boundary conditions. For this reason, spectral methods are necessary to discern its character.

The analysis begins with the superposition of the baseflow at leading order and the hydrodynamic wave taken as a first-order perturbation,

$$\tilde{M} = M + \check{m} \tag{15}$$

In terms of derivative operators, the following detail will conceptually outline the derivation of a linear relation from the nonlinear Navier-Stokes equations. The complete set of equations can be represented in terms of a nonlinear operator $\mathcal{N}$, such that the condition on $\check{m}$ may be deduced, starting with the total variable: [30]

$$\mathcal{N}(\tilde{M}) = 0 \rightarrow \mathcal{N}(M + \check{m}) = 0 \tag{16}$$

This representation requires a known solution for the baseflow, be it analytical or computational, that will satisfy

$$\mathcal{N}(M) = 0 \tag{17}$$

The expansion of Eq. (17) yields both linear and nonlinear parts according to

$$\mathcal{N}(M + \check{m}) = \mathcal{N}(M) + \mathcal{L}(M) \cdot \check{m} + \mathcal{O}(\check{m}^2) = 0 \tag{18}$$

Thus we identify the *linear* operator, $\mathcal{L}(M)$, acting on $\check{m}$. Given that $\mathcal{N}(M) = 0$ and that terms of $\mathcal{O}(\check{m}^2)$ are truncated, we are left only with the first-order equation for the hydrodynamic fluctuation, specifically

$$\mathcal{L}(M) \cdot \check{m} = 0 \tag{19}$$

Applying this notion to the complete viscous, incompressible Navier-Stokes equations gives rise to the *Linearized Navier-Stokes (LNS)* equations. This hydrodynamic LNS system can be expressed in term of instantaneous variables using

Continuity:

$$\frac{\partial \tilde{U}_r}{\partial r} + \frac{\tilde{U}_r}{r} + \frac{1}{r}\frac{\partial \tilde{U}_\theta}{\partial \theta} + \frac{\partial \tilde{U}_z}{\partial z} = 0 \tag{20a}$$

Radial momentum:

$$\frac{\partial \tilde{U}_r}{\partial t} + \tilde{U}_r\frac{\partial \tilde{U}_r}{\partial r} + \frac{\tilde{U}_\theta}{r}\frac{\partial \tilde{U}_r}{\partial \theta} - \frac{\tilde{U}_\theta^2}{r} + \tilde{U}_z\frac{\partial \tilde{U}_r}{\partial z} + \frac{\partial \tilde{P}}{\partial r} = \frac{1}{Re}\left(\frac{\partial^2 \tilde{U}_r}{\partial r^2} + \frac{1}{r}\frac{\partial \tilde{U}_r}{\partial r} - \frac{\tilde{U}_r}{r^2} + \frac{1}{r^2}\frac{\partial^2 \tilde{U}_r}{\partial \theta^2} - \frac{2}{r^2}\frac{\partial \tilde{U}_\theta}{\partial \theta} + \frac{\partial^2 \tilde{U}_r}{\partial z^2}\right) \tag{20b}$$

[‡] In this context, 'steady' is synonymous with non-oscillatory. The flow can be consistently varying in time but is considered steady since the temporal variation of the perturbation is much faster than the baseflow.

Tangential momentum:

$$\frac{\partial \tilde{U}_\theta}{\partial t} + \tilde{U}_r\frac{\partial \tilde{U}_\theta}{\partial r} + \frac{\tilde{U}_\theta}{r}\frac{\partial \tilde{U}_\theta}{\partial \theta} + \frac{\tilde{U}_r\tilde{U}_\theta}{r} + \tilde{U}_z\frac{\partial \tilde{U}_\theta}{\partial z} + \frac{1}{r}\frac{\partial \tilde{P}}{\partial \theta} = \frac{1}{Re}\left(\frac{\partial^2 \tilde{U}_\theta}{\partial r^2} + \frac{1}{r}\frac{\partial \tilde{U}_\theta}{\partial r} - \frac{\tilde{U}_\theta}{r^2} + \frac{1}{r^2}\frac{\partial^2 \tilde{U}_\theta}{\partial \theta^2} + \frac{2}{r^2}\frac{\partial \tilde{U}_r}{\partial \theta} + \frac{\partial^2 \tilde{U}_\theta}{\partial z^2}\right) \quad (20c)$$

Axial momentum:

$$\frac{\partial \tilde{U}_z}{\partial t} + \tilde{U}_r\frac{\partial \tilde{U}_z}{\partial r} + \frac{\tilde{U}_\theta}{r}\frac{\partial \tilde{U}_z}{\partial \theta} + \tilde{U}_z\frac{\partial \tilde{U}_z}{\partial z} + \frac{\partial \tilde{P}}{\partial z} = \frac{1}{Re}\left(\frac{\partial^2 \tilde{U}_z}{\partial r^2} + \frac{1}{r}\frac{\partial \tilde{U}_z}{\partial r} + \frac{1}{r^2}\frac{\partial^2 \tilde{U}_z}{\partial \theta^2} + \frac{\partial^2 \tilde{U}_z}{\partial z^2}\right) \quad (20d)$$

These equations are then perturbed by expressing the instantaneous velocity as a linear sum of the baseflow and a fluctuation attributed to the hydrodynamic wave. As per Eq. (15), since the collection of terms at $O(M)$ is identically zero, it is dismissed hereafter. Then, truncating terms of $O(\breve{m}^2)$ results in the appropriate first-order, linear stability equations. These are:

Continuity:

$$\frac{\partial \breve{u}_r}{\partial r} + \frac{\breve{u}_r}{r} + \frac{1}{r}\frac{\partial \breve{u}_\theta}{\partial \theta} + \frac{\partial \breve{u}_z}{\partial z} = 0 \quad (21a)$$

Radial momentum:

$$\frac{\partial \breve{u}_r}{\partial t} + U_r\frac{\partial \breve{u}_r}{\partial r} + \breve{u}_r\frac{\partial U_r}{\partial r} + \frac{U_\theta}{r}\frac{\partial \breve{u}_r}{\partial \theta} + \frac{\breve{u}_\theta}{r}\frac{\partial U_r}{\partial \theta} - \frac{2U_\theta\breve{u}_\theta}{r} + U_z\frac{\partial \breve{u}_r}{\partial z} + \breve{u}_z\frac{\partial U_r}{\partial z} + \frac{\partial \breve{p}}{\partial r} = \varepsilon\left(\frac{\partial^2 \breve{u}_r}{\partial r^2} + \frac{1}{r}\frac{\partial \breve{u}_r}{\partial r} - \frac{\breve{u}_r}{r^2} + \frac{1}{r^2}\frac{\partial^2 \breve{u}_r}{\partial \theta^2} - \frac{2}{r^2}\frac{\partial \breve{u}_\theta}{\partial \theta} + \frac{\partial^2 \breve{u}_r}{\partial z^2}\right) \quad (21b)$$

Tangential momentum:

$$\frac{\partial \breve{u}_\theta}{\partial t} + U_r\frac{\partial \breve{u}_\theta}{\partial r} + \breve{u}_r\frac{\partial U_\theta}{\partial r} + \frac{U_\theta}{r}\frac{\partial \breve{u}_\theta}{\partial \theta} + \frac{\breve{u}_\theta}{r}\frac{\partial U_\theta}{\partial \theta} + \frac{U_r\breve{u}_\theta}{r} + \frac{\breve{u}_r U_\theta}{r} + U_z\frac{\partial \breve{u}_\theta}{\partial z} + \breve{u}_z\frac{\partial U_\theta}{\partial z} + \frac{1}{r}\frac{\partial \breve{p}}{\partial \theta} = \varepsilon\left(\frac{\partial^2 \breve{u}_\theta}{\partial r^2} + \frac{1}{r}\frac{\partial \breve{u}_\theta}{\partial r} - \frac{\breve{u}_\theta}{r^2} + \frac{1}{r^2}\frac{\partial^2 \breve{u}_\theta}{\partial \theta^2} + \frac{2}{r^2}\frac{\partial \breve{u}_r}{\partial \theta} + \frac{\partial^2 \breve{u}_\theta}{\partial z^2}\right) \quad (21c)$$

Axial momentum:

$$\frac{\partial \breve{u}_z}{\partial t} + U_r\frac{\partial \breve{u}_z}{\partial r} + \breve{u}_r\frac{\partial U_z}{\partial r} + \frac{U_\theta}{r}\frac{\partial \breve{u}_z}{\partial \theta} + \frac{\breve{u}_\theta}{r}\frac{\partial U_z}{\partial \theta} + U_z\frac{\partial \breve{u}_z}{\partial z} + \breve{u}_z\frac{\partial U_z}{\partial z} + \frac{\partial \breve{p}}{\partial z} = \varepsilon\left(\frac{\partial^2 \breve{u}_z}{\partial r^2} + \frac{1}{r}\frac{\partial \breve{u}_z}{\partial r} + \frac{1}{r^2}\frac{\partial^2 \breve{u}_z}{\partial \theta^2} + \frac{\partial^2 \breve{u}_z}{\partial z^2}\right) \quad (21d)$$

IV. On the Parallel Flow Assumption

In an insightful study by Casalis and Vuillot,[30] the validity of the normal mode assumption is discussed, namely, the traditional one-dimensional statement,

$$\breve{m}(r,\theta,z,t) = m(r)\exp\left[i\left(q\theta + \alpha z - \omega t\right)\right] \quad (22)$$

and its applicability to two-dimensional baseflows. Since continuity requires a dependence of the streamwise velocity on the streamwise coordinate through the nonzero transverse velocity, $\frac{\partial \breve{u}_z}{\partial z} = -\frac{\partial \breve{u}_r}{\partial r} - \frac{\breve{u}_r}{r} - \frac{1}{r}\frac{\partial \breve{u}_\theta}{\partial \theta}$, two-dimensional flows exhibit *nonparallel* effects. Therefore, the normal mode remains a valid approximation only for flows that are weakly dependent on the streamwise coordinate, or

$$\frac{\partial M}{\partial z}, \frac{\partial M}{\partial \theta} \ll \frac{\partial M}{\partial r} \quad (23)$$

This inequality establishes the *parallel flow assumption*. In fact, setting the left-hand-side of this equality equal to zero may be viewed as the basis for deriving the Orr-Sommerfeld equation.

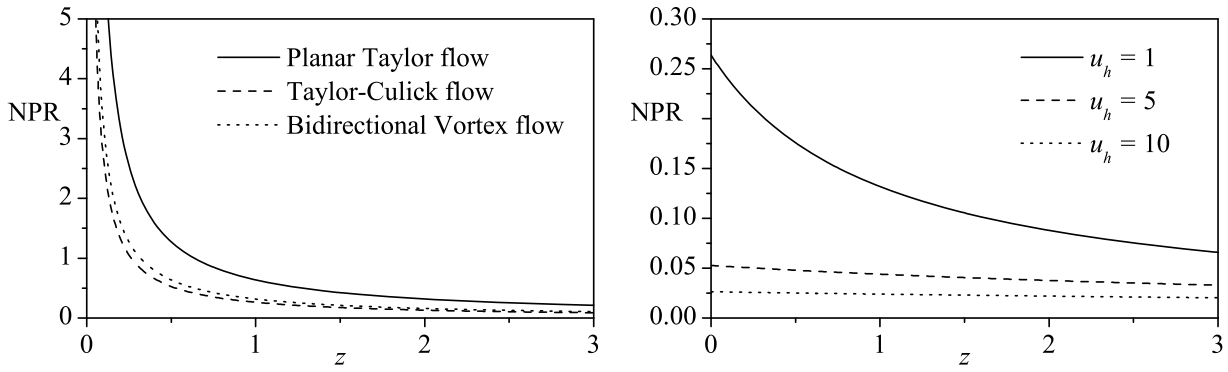

a) Three common baseflows

b) Taylor-Culick flow with uniform headwall injection[32]

Figure 5. A qualitative comparison of the nonparallel effects for several baseflows for $r = 0.5$.

Casalis and Vuillot[30] go further to propose a means of analyzing the degree by which the parallel flow assumption is violated. Since the degree of nonparallelism is related to the magnitude of the transverse velocity with respect to its streamwise companion, we can simply calculate their ratio to gauge their significance. To illustrate this point, the Nonparallel Ratio (NPR) is evaluated for several baseflows that give

$$\mathrm{NPR_T} = \left|\frac{-\sin(\pi r/2)}{\pi z/2\cos(\pi r/2)}\right| \approx \frac{r}{z} + \frac{\pi^2 r^3}{12z} + O(r^5) \qquad \text{Planar Taylor flow}[30] \qquad (24a)$$

$$\mathrm{NPR_{TC}} = \left|\frac{-1/r\sin(\pi r^2/2)}{\pi z\cos(\pi r^2/2)}\right| \approx \frac{r}{2z} + O(r^5) \qquad \text{Axisymmetric Taylor-Culick flow}[31] \qquad (24b)$$

$$\mathrm{NPR_{CL}} = \left|\frac{-\kappa/r\sin(\pi r^2)}{2\pi\kappa z\cos(\pi r^2)}\right| \approx \frac{r}{2z} + O(r^5) \qquad \text{Bidirectional Vortex flow}[15] \qquad (24c)$$

$$\mathrm{NPR_{TCH}} = \left|\frac{-1/r\sin(\pi r^2/2)}{\pi(z+u_h)\cos(\pi r^2/2)}\right| \approx \frac{r}{2(z+u_h)} + O(r^5) \qquad \text{Taylor-Culick with headwall injection}[32] \qquad (24d)$$

Equations (24a–24d) exhibit one common characteristic: their NPR $\approx z^{-1}$ becomes large near the headwall. This effect is mitigated by the inclusion of headwall injection for Eq. (24d). Clearly, a large u_h helps to maintain a small NPR as $z \to 0$. In long chambers, the value of $1/z$ diminishes along with the nonparallel effects when sufficiently removed from the headwall to the extent of justifying the use of the LNP approach. In contrast, short chambers, such as those associated with bidirectional vortex motion, are especially susceptible to nonparallel effects. This behavior may be graphically verified through Fig. 5a where the NPR of several propulsion-related baseflows are featured. Unlike the Taylor-family of solutions for which $z + u_h$ extends between 25 and 100 (SRMs or hybrids with headwall injection), bidirectional vortex configurations typically extend over $0 \leq z \leq 5$. The portion of this range in which the NPR remains large is not negligible, hence warranting the use of the biglobal stability approach.

In seeking a biglobal stability solution, we eliminate the deficiencies of the parallel flow assumption while simultaneously increasing the algebraic manipulations entailed in the ensuing formulations and the required computational time. Given an axisymmetric, two-dimensional baseflow, these solutions must consider both the transverse and streamwise coordinates.

V. Deriving the Cylindrical Biglobal Stability Equations

In general, the derivation of the biglobal stability equations resembles that of the LNP approach with the exception of using a two-dimensional, biglobal, normal mode rather than the traditional one-dimensional function. In this case, we begin with Eqs. (21a–21d) and consider a two-dimensional modal ansatz of the form

$$\breve{m} = m(r,z)\exp\left[i\left(q\theta - \omega t\right)\right] \qquad (25)$$

The criteria for parallel flow are now modified to include streamwise variations. Here we use

$$\frac{\partial M}{\partial \theta} \ll \frac{\partial M}{\partial r} \quad \text{and} \quad \frac{\partial M}{\partial \theta} \ll \frac{\partial M}{\partial z} \tag{26}$$

This assumption warrants a baseflow that is axisymmetric or nearly axisymmetric.[23] The inequalities of Eq. (26) require that the baseflow be periodic with respect to θ. In the limit as $\partial M/\partial z \to 0$, the one-dimensional normal mode equations are recovered.

To make progress, we apply the biglobal ansatz systematically to the extent of retrieving the general biglobal stability equations for this class of problems. After some effort, we extract

Continuity:

$$\frac{\partial u_r}{\partial r} + \frac{u_r}{r} + iq\frac{u_\theta}{r} + \frac{\partial u_z}{\partial z} = 0 \tag{27a}$$

Radial momentum:

$$\begin{aligned} -i\omega u_r + U_r\frac{\partial u_r}{\partial r} + u_r\frac{\partial U_r}{\partial r} + iq\frac{U_\theta u_r}{r} + \frac{u_\theta}{r}\frac{\partial U_r}{\partial \theta} - \frac{2U_\theta u_\theta}{r} + U_z\frac{\partial u_r}{\partial z} + u_z\frac{\partial U_r}{\partial z} + \frac{\partial p}{\partial r} \\ = \varepsilon\left(\frac{\partial^2 u_r}{\partial r^2} + \frac{1}{r}\frac{\partial u_r}{\partial r} - \frac{u_r}{r^2} - \frac{q^2}{r^2}u_r - \frac{2iq}{r^2}u_\theta + \frac{\partial^2 u_r}{\partial z^2}\right) \end{aligned} \tag{27b}$$

Tangential momentum:

$$\begin{aligned} -i\omega u_\theta + U_r\frac{\partial u_\theta}{\partial r} + u_r\frac{\partial U_\theta}{\partial r} + iq\frac{U_\theta u_\theta}{r} + \frac{u_\theta}{r}\frac{\partial U_\theta}{\partial \theta} + \frac{U_r u_\theta}{r} + \frac{u_r U_\theta}{r} + U_z\frac{\partial u_\theta}{\partial z} + u_z\frac{\partial U_\theta}{\partial z} + iq\frac{p}{r} \\ = \varepsilon\left(\frac{\partial^2 u_\theta}{\partial r^2} + \frac{1}{r}\frac{\partial u_\theta}{\partial r} - \frac{u_\theta}{r^2} - \frac{q^2}{r^2}u_\theta + \frac{2iq}{r^2}u_r + \frac{\partial^2 u_\theta}{\partial z^2}\right) \end{aligned} \tag{27c}$$

Axial momentum:

$$\begin{aligned} -i\omega u_z + U_r\frac{\partial u_z}{\partial r} + u_r\frac{\partial U_z}{\partial r} + iq\frac{U_\theta u_z}{r} + \frac{u_\theta}{r}\frac{\partial U_z}{\partial \theta} + U_z\frac{\partial u_z}{\partial z} + u_z\frac{\partial U_z}{\partial z} + \frac{\partial p}{\partial z} \\ = \varepsilon\left(\frac{\partial^2 u_z}{\partial r^2} + \frac{1}{r}\frac{\partial u_z}{\partial r} - \frac{q^2}{r^2}u_z + \frac{\partial^2 u_z}{\partial z^2}\right) \end{aligned} \tag{27d}$$

Since many baseflows are two-dimensional, it may be preferable to express these equations in terms of the streamfunction. A streamfunction formulation has distinct advantages, the first being the reduced computational requirements of a single dependent variable in lieu of four. Chedevergne [33] shows how differentiating and summing the streamfunction equations can eliminate the pressure terms. However, by keeping the present velocity-pressure formulation, we are able to develop an algorithm that can handle not only two-dimensional flows, but also three-dimsional, axisymmetric representations. A similar construction of the biglobal stability equations in Cartesian coordinates is discussed by Robitaillié-Montané and Casalis.[34]

VI. On the Choice of Chebyshev Spectral Collocation

Given the resulting linear PDEs in Eq. (27), an efficient type of collocation is required. The type of polynomial collocation is driven by the need to control the localized grid resolution, numerical stability, and overall accuracy. Algebraic polynomials (Power or Maclaurin series) can be constructed in a variety of ways including Lagrange polynomials, Newton divided differences, Padé approximations, or even straightforward Taylor series expansions of known functions.[35] Trigonometric polynomial interpolators and other orthogonal polynomials, such as the set of Chebyshev or Legendre polynomials, can be advantageous for analytical problems involving quadrature and differential equations. Their nonuniformly spaced grid schemes are often useful in discretizing boundary layers because of their ability to impose a fine grid space near the wall and a coarse grid elsewhere. Furthermore, there are distinct advantages of using nonuniformly spaced interpolating points over equally-spaced points. Equally spaced points tend toward the well known Gibbs phenomenon for Fourier spectral methods and the Runge phenomenon [36] for algebraic methods such as Lagrange interpolation.[35] Figure 6 reproduces the example by Trefethen[36] where the deficiencies of equally spaced, algebraic polynomial interpolation are shown and contrasted to the Chebyshev collocation that clearly leads to improved accuracy.

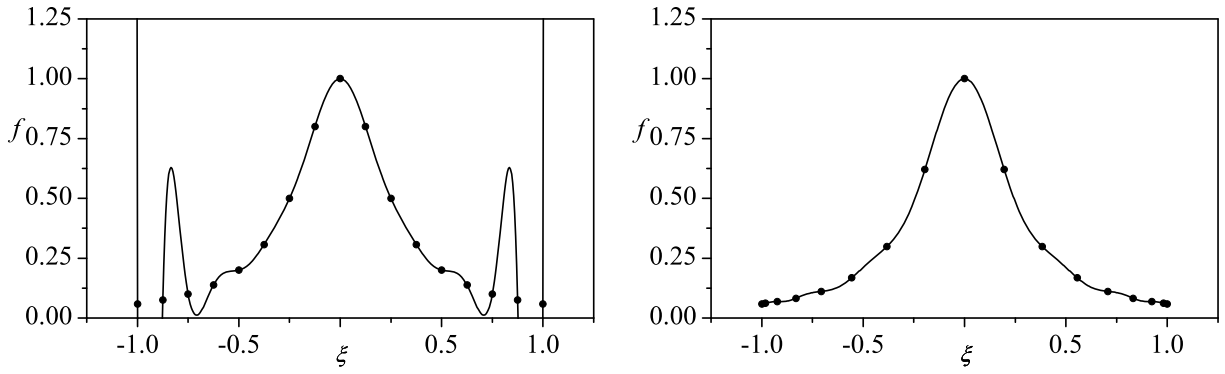

Figure 6. Comparison between interpolation with a) equally spaced and b) Chebyshev grids. The Runge phenomenon can be easily seen in Part a).

A. Chebyshev Polynomials

Chebyshev polynomials of the first type satisfy the equation

$$(1-\xi^2)T''_{N-1}(\xi) - \xi T'_{N-1}(\xi) + N^2 T_{N-1}(\xi) = 0 \tag{28}$$

The solution to Eq. (28) can benefit from the following variable transformation:

$$\xi = \cos\theta \quad \text{with} \quad \frac{\mathrm{d}}{\mathrm{d}\xi} = -\frac{1}{\sin\theta}\frac{\mathrm{d}}{\mathrm{d}\theta} \tag{29}$$

thus resulting in a differential equation of the form

$$\begin{cases} \dfrac{\mathrm{d}^2 T_{N-1}}{\mathrm{d}\theta^2} + (N-1)^2 T_{N-1} = 0 \\ T_{N-1}(\theta) = \cos[(N-1)\theta] = \cos\left[(N-1)\arccos\xi\right] \end{cases} \tag{30}$$

It can be seen that Chebyshev polynomials are orthogonal. This statement has been shown to only be true over the interval $[-1, 1]$.[37] It is also necessary to express the general derivative formula for these polynomials. Using

$$T_{N-1}(\xi) = T_{N-1}(\cos\theta) = \cos[(N-1)\theta]; \quad \forall\theta \tag{31}$$

differentiation with respect to θ yields

$$\frac{\mathrm{d}T_{N-1}}{\mathrm{d}\theta} = -T'_{N-1}(\cos\theta)\sin\theta = -(N-1)\sin[(N-1)\theta] \tag{32}$$

Equation (32) enables us to solve for T'_{N-1}, namely,

$$T'_{N-1}(\theta) = (N-1)\frac{\sin[(N-1)\theta]}{\sin\theta} \quad \text{for} \quad N = 1, 2, 3... \quad \text{with} \quad \theta = \arccos\xi \tag{33}$$

This result is necessary to obtain the Chebyshev polynomial weight function.

B. Chebyshev Discretization

The Chebyshev polynomials can be used to approximate known and unknown functions to degree N. If we define the exact polynomial representation of degree infinity of a function $f(\xi)$ as $\mathcal{P}_\infty f(\xi_\infty)$, then a discrete polynomial of order N may be written as

$$\mathcal{P}_N f(\xi) = \sum_{i=1}^{N} f(\xi_i)\lambda_i(\xi) \tag{34}$$

where the sequence $\{\xi_i\}$ encompasses the collocation points for $i = 1, \ldots, N$ and $\lambda_i(\xi)$ represents the i^{th} weight function. For Chebyshev polynomials,

$$\lambda_i(\xi) = (-1)^i \left(\frac{1-\xi^2}{\xi - \xi_i}\right)\left[\frac{T'_{N-1}(\theta)}{d_i(N-1)^2}\right] \quad \text{with} \quad \begin{cases} \xi_i = \cos\left[\frac{(i-1)\pi}{N-1}\right] \\ \theta = \arccos\xi \end{cases} \tag{35}$$

where

$$d_i = \begin{cases} 2; & i = 1 \text{ or } N \\ 1; & \text{otherwise} \end{cases} \tag{36}$$

This discretization scheme leads to a system of N equations and N unknowns to be solved simultaneously for the discrete values of the spectral function $f(\xi_i)$. The polynomials are constructed from the weight functions multiplied by the functional value at each of the collocation points. Analytically, this framework is not reasonable for high resolution grids, although it is well suited for numerical computation. In fact, any number of linear algebraic solvers can be employed. Although time consuming for large systems, Gaussian elimination is the most popular technique. Fortunately, the algorithm **chebint** provided by Weideman and Reddy [38] can interpolate a coarse solution over a finer grid.

Recalling that our polynomial representation is defined as $\mathcal{P}_N f(\xi)$, the first derivative of f may be approximated at the collocation nodes $\xi_1, \ldots, \xi_N$ with the exact first derivative of $\mathcal{P}_N f(\xi)$. The polynomial representation of the derivative is defined as

$$\mathcal{D}_N f(\xi) = [\mathcal{P}_N f(\xi)]' \tag{37}$$

The associated error is of the exponential type and depends on the smoothness of the original function $f(\xi_i)$.[39] The derivative can therefore be defined as the polynomial

$$\mathcal{D}_N f(\xi) = \sum_{i=1}^{N} f(\xi_i)\lambda'_i(\xi) \tag{38}$$

The derivative of the weight functions, $\lambda'_i(\xi)$, can be calculated *a priori* and stored in the *pseudo-spectral differentiation matrix*, D, where $D_{ij} = \lambda'_j(\xi_i)$ for $i, j = 1, \ldots, N$. Finally, knowing the differential matrix leads us to write the derivative of a function spectrally as

$$f'(\xi_i) = D_N f(\xi_i) \tag{39}$$

Equation (39) offers a differentiation matrix that is unique to each collocation method employed. By differentiating the N^{th} order Chebyshev polynomial and resolving the coefficients at 1 through N collocation points, a general formula for the differentiation matrix may be deduced. This was first shown by Voight, Gottlieb and Hussaini [40] and is now presented as Theorem 1.

Theorem 1. Chebyshev Differentiation Matrix. *For each $N \geq 1$, let the rows and columns of the $(N+1) \times (N+1)$ Chebyshev spectral differentiation matrix D_N be indexed from 0 to N. The entries of this matrix are:*

$$D_N = \begin{cases} (D_N)_{11} = \dfrac{2(N-1)^2 + 1}{6} & \\ (D_N)_{ii} = \dfrac{-\xi_i}{2\left(1-\xi_i^2\right)} & i = 2, \ldots, N-1 \\ (D_N)_{ij} = \dfrac{d_i}{d_j}\dfrac{(-1)^{i+j}}{\left(\xi_i - \xi_j\right)} & i \neq j, \quad i, j = 2, \ldots, N-1 \\ (D_N)_{NN} = -\dfrac{2(N-1)^2 + 1}{6} & \end{cases} \tag{40}$$

In the interest of clarity, the corresponding matrix elements may be depicted graphically using

$$D_N = \left(\begin{array}{c|ccc|c} \frac{2(N-1)^2+1}{6} & \cdots & \frac{2(-1)^{1+j}}{1-\xi_j} & \cdots & \frac{1}{2}(-1)^{1+N} \\ \hline \vdots & \ddots & \cdots & \frac{(-1)^{i+j}}{\xi_i-\xi_j} & \vdots \\ \frac{1}{2}\frac{(-1)^{i+1}}{\xi_i-1} & \vdots & \frac{-\xi_j}{2(1-\xi_j^2)} & \vdots & \frac{1}{2}\frac{(-1)^{i+N}}{\xi_i+1} \\ \vdots & \frac{(-1)^{i+j}}{\xi_i-\xi_j} & \cdots & \ddots & \vdots \\ \hline -\frac{1}{2}(-1)^{N+1} & \cdots & -\frac{2(-1)^{N+j}}{1+\xi_j} & \cdots & -\frac{2(N-1)^2+1}{6} \end{array}\right) \tag{41}$$

Higher-order derivatives may be computed by simply raising the first-order, pseudo-spectral differentiation matrix to the corresponding power

$$\begin{cases} \frac{\mathrm{d}}{\mathrm{d}\xi} & \longrightarrow D_N \\ \frac{\mathrm{d}^2}{\mathrm{d}\xi^2} & \longrightarrow (D_N)^2 = D_N \times D_N \\ \vdots & \\ \frac{\mathrm{d}^n}{\mathrm{d}\xi^n} & \longrightarrow (D_N)^n = \underbrace{D_N \times D_N \times \ldots \times D_N}_{\times n} \end{cases} \tag{42}$$

Computationally, this operation costs $O(N^{3n})$ flops. Higher-order spectral derivatives can also be evaluated through either recurrence relations [41,42] or formulas [43] that reduce the computational cost to $O(N^{2n})$. However, since this operation needs to be computed only once and stored for later use, the former operation remains sufficient here.

The collection of spectral differentiation and integration codes detailed in the article by Weideman and Reddy [38] has become an invaluable tool for those undertaking spectral analysis in MATLAB. The function **chebdif** generates N collocation points and the n^{th} order pseudo-spectral Chebyshev differentiation matrix over the interval $[-1, 1]$. Mapping can be applied to account for different domains.

C. Tensor Product Grids

At this stage, it may be instructive to note that a two-dimensional problem requires a two-dimensional grid based on directionally independent Chebyshev points. Such a grid is called a tensor product grid [36] and can allow for two independent variables to coexist in the same matrix operator.

Tensor product grids require the use of *Kronecker products*. The Kronecker product of two matrices is denoted by $A_{ij} \otimes B_{mn} = C_{i\times m\ j\times n}$ where $C_{i\times m\ j\times n}$ is a block matrix such that each block is built with $a_{ij}B_{mn}$. For the sake of clarity, the Kronecker product is given by

$$A_{ij} \otimes B_{mn} = \begin{pmatrix} a_{11}B_{mn} & \cdots & a_{1j}B_{mn} \\ \vdots & \ddots & \vdots \\ a_{i1}B_{mn} & \cdots & a_{jj}B_{mn} \end{pmatrix} \tag{43}$$

so that each element of A_{ij} is multiplied by the entire matrix B_{mn}. This operation may be evaluated in MATLAB with the command **kron**(X,Y).

D. Domain Mapping

For a multidimensional partial differential equation, each independent variable must be mapped over the interval $[-1, 1]$. In the two-dimensional case illustrated here, we define two general mapping relations:

$$\begin{cases} r = \dfrac{B}{2}(\xi+1) - \dfrac{A}{2}(\xi-1) & \longleftrightarrow \quad \xi = \dfrac{2r-(B+A)}{B-A} \\ z = \dfrac{D}{2}(\eta+1) - \dfrac{C}{2}(\eta-1) & \longleftrightarrow \quad \eta = \dfrac{2z-(D+C)}{D-C} \end{cases} \quad \text{and so} \quad \begin{cases} \dfrac{\partial}{\partial r} = \dfrac{2}{B-A}\dfrac{\partial}{\partial \xi} \\ \dfrac{\partial}{\partial z} = \dfrac{2}{D-C}\dfrac{\partial}{\partial \eta} \end{cases} \tag{44}$$

where (A, B) and (C, D) are the bounds on r and z, respectively.

The Kronecker product may be used to build a single operator matrix out of the collocation in two directions. Accordingly, derivatives with respect to η take the form $(I_N) \otimes (D_N)^n$ while derivatives with respect to ξ transform into $(D_N)^n \otimes (I_N)$, where (I_N) is the $N \times N$ identity matrix.

We see in Fig. 7 that these matrices are sparse but not so sparse that we must resort to special methods for singular or sparse matrices. The inclusion of boundary conditions increases their sparsity but only around the outer perimeter. In the case of eigenvalue problems, their block matrix character can be decomposed to accelerate convergence. [39] Finite element discretization would result in substantially more sparse matrices. It would also require hundreds or thousands of collocation points, whereas Chebyshev collocation and Kronecker products require tens to hundreds of points for an accurate resolution. [36]

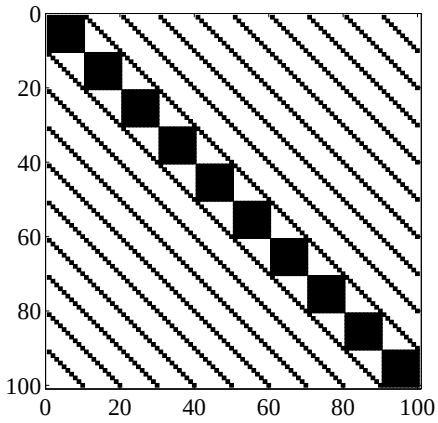

Figure 7. The location of nonzero elements in the product tensor matrix with no boundary conditions.

VII. Deriving the Spectral Biglobal Equations

Having reviewed the foundational aspects of this analysis, we now return to the biglobal stability equations derived in Sec. V. Being interested in the spectral decomposition and eigensolution of this problem, we formulate the system in terms of the generalized eigenvalue problem:

$$A_{ij} f_i = \lambda B_{ij} f_i \tag{45}$$

To do so, we build the operator matrices, A_{ij} and B_{ij}, from smaller $N^2 \times N^2$ block matrices (e.g. A_{c,u_r}). Each block matrix refers to the operator of a specific dependent variable in one of the four governing equations. A general block

diagram is furnished below:

$$A_{ij} = \begin{array}{r} \\ \text{Cont.} \\ r-\text{mom.} \\ \theta-\text{mom.} \\ z-\text{mom.} \end{array} \begin{array}{c} \begin{array}{cccc} u_r(r) & u_\theta(r) & u_z(r) & p(r) \\ \downarrow & \downarrow & \downarrow & \downarrow \end{array} \\ \left[\begin{array}{c|c|c|c} A_{c,u_r} & A_{c,u_\theta} & A_{c,u_z} & A_{c,p} \\ \hline A_{r,u_r} & A_{r,u_\theta} & A_{r,u_z} & A_{r,p} \\ \hline A_{\theta,u_r} & A_{\theta,u_\theta} & A_{\theta,u_z} & A_{\theta,p} \\ \hline A_{z,u_r} & A_{z,u_\theta} & A_{z,u_z} & A_{z,p} \end{array}\right] \end{array}$$

$$B_{ij} = \begin{array}{r} \\ \text{Cont.} \\ r-\text{mom.} \\ \theta-\text{mom.} \\ z-\text{mom.} \end{array} \begin{array}{c} \\ \left[\begin{array}{c|c|c|c} B_{c,u_r} & B_{c,u_\theta} & B_{c,u_z} & B_{c,p} \\ \hline B_{r,u_r} & B_{r,u_\theta} & B_{r,u_z} & B_{r,p} \\ \hline B_{\theta,u_r} & B_{\theta,u_\theta} & B_{\theta,u_z} & B_{\theta,p} \\ \hline B_{z,u_r} & B_{z,u_\theta} & B_{z,u_z} & B_{z,p} \end{array}\right] \end{array}$$

This implies that the final matrices are $4N^2 \times 4N^2$. The comparable one-dimensional problem would only be $4N \times 4N$ since it does not require the use of a product tensor grid. Clearly, the biglobal problem will incur a significant increase in computational power to render solutions at the same resolution as the one-dimensional approach. Fortuitously, the efforts by Chedevergne [33] and Theofilis [23] lead us to believe that as much as an order of magnitude fewer collocation points can be used for each independent variable to achieve convergence to a viable solution. [23,33] In the present study, we find that the use of $N = 50$ leads to a reasonable solution.

In the interest of clarity, it is important to express the governing equations in operator form. These are given by

Continuity:

$$\left(\frac{\partial}{\partial r} + r^{-1}\right) u_r + \left(iqr^{-1}\right) u_\theta + \left(\frac{\partial}{\partial z}\right) u_z = 0 \tag{46a}$$

Radial momentum:

$$\left\{U_r \frac{\partial}{\partial r} + \frac{\partial U_r}{\partial r} + iqU_\theta r^{-1} + U_z \frac{\partial}{\partial z} - \varepsilon\left[\frac{\partial^2}{\partial r^2} + r^{-1}\frac{\partial}{\partial r} - \left(1+q^2\right)r^{-2} + \frac{\partial^2}{\partial z^2}\right]\right\} u_r + \left(2iq\varepsilon r^{-2} - 2U_\theta r^{-1} + r^{-1}\frac{\partial U_r}{\partial \theta}\right) u_\theta + \left(\frac{\partial U_r}{\partial z}\right) u_z + \left(\frac{\partial}{\partial r}\right) p = (i\omega)\, u_r \tag{46b}$$

Tangential momentum:

$$\left(\frac{\partial U_\theta}{\partial r} + U_\theta r^{-1} - 2iq\varepsilon r^{-2}\right) u_r + \left\{U_r \frac{\partial}{\partial r} + U_r r^{-1} + iqU_\theta r^{-1} + r^{-1}\frac{\partial U_\theta}{\partial \theta} + U_z \frac{\partial}{\partial z} - \varepsilon\left[\frac{\partial^2}{\partial r^2} + r^{-1}\frac{\partial}{\partial r} - \left(1+q^2\right)r^{-2} + \frac{\partial^2}{\partial z^2}\right]\right\} u_\theta + \left(\frac{\partial U_\theta}{\partial z}\right) u_z + \left(iqr^{-1}\right) p = (i\omega)\, u_\theta \tag{46c}$$

Axial momentum:

$$\left(\frac{\partial U_z}{\partial r}\right) u_r + \left(r^{-1}\frac{\partial U_z}{\partial \theta}\right) u_\theta + \left[U_r \frac{\partial}{\partial r} + iqU_\theta r^{-1} + \frac{\partial U_z}{\partial z} + U_z \frac{\partial}{\partial z} - \varepsilon\left(\frac{\partial^2}{\partial r^2} + r^{-1}\frac{\partial}{\partial r} - q^2 r^{-2} + \frac{\partial^2}{\partial z^2}\right)\right] u_z + \left(\frac{\partial}{\partial z}\right) p = (i\omega)\, u_z \tag{46d}$$

Next, the domain must be transformed for both the r and z coordinates. For arbitrary chamber length, we take the domain to be $0 \le r \le 1$ and $0 \le z \le Z_N$. Referring to Eq. (44) for a two-dimensional mapping relation, we find

$$\begin{cases} r = \dfrac{1}{2}(\xi + 1) & \longleftrightarrow \quad \xi = 2r - 1 \\ z = \dfrac{Z_N}{2}(\eta + 1) & \longleftrightarrow \quad \eta = \dfrac{2z - Z_N}{Z_N} \end{cases} \quad \text{and} \quad \begin{cases} \dfrac{\partial}{\partial r} = 2\dfrac{\partial}{\partial \xi} \\ \dfrac{\partial}{\partial z} = \dfrac{2}{Z_N}\dfrac{\partial}{\partial \eta} \end{cases} \tag{47}$$

Subsequently, the block matrices become

$$\begin{cases} A_{c,u_r} &= \bar{D}^r_N + r^{-1}_{ii} \\ A_{c,u_\theta} &= iqr^{-1}_{ii} \\ A_{c,u_z} &= \bar{D}^z_N \\ A_{c,p} &= 0 \end{cases} \qquad \begin{cases} B_{c,u_r} &= 0 \\ B_{c,u_\theta} &= 0 \\ B_{c,u_z} &= 0 \\ B_{c,p} &= 0 \end{cases} \tag{48}$$

$$\begin{cases} A_{r,u_r} &= U_{rii}\bar{D}^r_N + \left(\dfrac{\partial U_r}{\partial r}\right)_{ii} + iqU_{\theta ii}r^{-1}_{ii} + U_{zii}\bar{D}^z_N \\ & \quad -\varepsilon\left[(\bar{D}^r_N)^2 + r^{-1}_{ii}\bar{D}^r_N - \left(1+q^2\right)r^{-2}_{ii} + (\bar{D}^z_N)^2\right] \\ A_{r,u_\theta} &= 2iq\varepsilon r^{-2}_{ii} - 2U_{\theta ii}r^{-1}_{ii} + r^{-1}_{ii}\left(\dfrac{\partial U_r}{\partial \theta}\right)_{ii} \\ A_{r,u_z} &= \left(\dfrac{\partial U_r}{\partial z}\right)_{ii} \\ A_{r,p} &= \bar{D}^r_N \end{cases} \qquad \begin{cases} B_{r,u_r} &= iI_N \\ B_{r,u_\theta} &= 0 \\ B_{r,u_z} &= 0 \\ B_{r,p} &= 0 \end{cases} \tag{49}$$

$$\begin{cases} A_{\theta,u_r} &= \left(\dfrac{\partial U_\theta}{\partial r}\right)_{ii} + U_{\theta ii}r^{-1}_{ii} - 2iq\varepsilon r^{-2}_{ii} \\ A_{\theta,u_\theta} &= U_{rii}\bar{D}^r_N + U_{rii}r^{-1}_{ii} + iqU_{\theta ii}r^{-1}_{ii} \\ & \quad + r^{-1}_{ii}\left(\dfrac{\partial U_\theta}{\partial \theta}\right)_{ii} + U_{zii}\bar{D}^z_N \\ & \quad -\varepsilon\left[(\bar{D}^r_N)^2 + r^{-1}_{ii}\bar{D}^r_N - \left(1+q^2\right)r^{-2}_{ii} + (\bar{D}^z_N)^2\right] \\ A_{\theta,u_z} &= \left(\dfrac{\partial U_\theta}{\partial z}\right)_{ii} \\ A_{\theta,p} &= iqr^{-1}_{ii} \end{cases} \qquad \begin{cases} B_{\theta,u_r} &= 0 \\ B_{\theta,u_\theta} &= iI_N \\ B_{\theta,u_z} &= 0 \\ B_{\theta,p} &= 0 \end{cases} \tag{50}$$

$$\begin{cases} A_{z,u_r} &= \left(\dfrac{\partial U_z}{\partial r}\right)_{ii} \\ A_{z,u_\theta} &= r^{-1}_{ii}\left(\dfrac{\partial U_z}{\partial \theta}\right)_{ii} \\ A_{z,u_z} &= U_{rii}\bar{D}^r_N + iqU_{\theta ii}r^{-1}_{ii} + \left(\dfrac{\partial U_z}{\partial z}\right)_{ii} + U_{zii}\bar{D}^z_N \\ & \quad -\varepsilon\left[(\bar{D}^r_N)^2 + r^{-1}_{ii}\bar{D}^r_N - q^2r^{-2}_{ii} + \bar{D}^z_N\right] \\ A_{z,p} &= \bar{D}^z_N \end{cases} \qquad \text{and, finally,} \qquad \begin{cases} B_{z,u_r} &= 0 \\ B_{z,u_\theta} &= 0 \\ B_{z,u_z} &= iI_N \\ B_{z,p} &= 0 \end{cases} \tag{51}$$

where the overbar implies that spectral operators are mapped to the physical domain, $0 \le r \le 1$ and $0 \le z \le Z_N$.

The boundary conditions for this system are taken to be those corresponding to the acoustic field in the chamber, $\boldsymbol{n}\cdot\boldsymbol{u} = 0$ and $\boldsymbol{n}\cdot\nabla p = 0$. The work by Chedevergne [33] uses a streamfunction formulation and requires comparable conditions. The more formal discussion by Robitaillié-Montané and Casalis [34] provides a formulation with a two-dimensional baseflow in Cartesian coordinates. It is therefore determined that for an eigenvalue problem in which the boundary conditions on the domain must be homogeneous, the axisymmetric system must be closed using

$$\begin{cases} u_r(0,z) &= 0 \\ u_r(1,z) &= 0 \\ u_r(r,0) &= 0 \\ u_r(r,Z_f) &= 0 \end{cases} \quad \begin{cases} u_\theta(0,z) &= 0 \\ u_\theta(1,z) &= 0 \\ u_\theta(r,0) &= 0 \\ u_\theta(r,Z_f) &= 0 \end{cases} \quad \begin{cases} \partial_r u_z(0,z) &= 0 \\ u_z(1,z) &= 0 \\ u_z(r,0) &= 0 \\ u_z(r,Z_f) &= 0 \end{cases} \quad \begin{cases} \partial_r p(0,z) &= 0 \\ \partial_r p(1,z) &= 0 \\ \partial_z p(r,0) &= 0 \\ \partial_z p(r,Z_f) &= 0 \end{cases} \tag{52}$$

The streamwise conditions on all velocities at the headwall are zeroed as a means of satisfying no-slip. At the endwall, the boundary conditions on velocity and pressure are selected in conformance with an acoustically closed chamber. Finally, centerline boundary conditions are defined to represent an axisymmetric flow.

The asymmetric analog of Eq. (52) may be written as

$$\left\{\begin{array}{lcl} u_r(0,z) &=& 0 \\ u_r(1,z) &=& 0 \\ u_r(r,0) &=& 0 \\ u_r(r,Z_f) &=& 0 \end{array}\right. \quad \left\{\begin{array}{lcl} u_\theta(0,z) &=& 0 \\ u_\theta(1,z) &=& 0 \\ u_\theta(r,0) &=& 0 \\ u_\theta(r,Z_f) &=& 0 \end{array}\right. \quad \left\{\begin{array}{lcl} \boldsymbol{u_z(0,z)} &\boldsymbol{=}& \boldsymbol{0} \\ u_z(1,z) &=& 0 \\ u_z(r,0) &=& 0 \\ u_z(r,Z_f) &=& 0 \end{array}\right. \quad \left\{\begin{array}{lcl} \boldsymbol{p(0,z)} &\boldsymbol{=}& \boldsymbol{0} \\ \partial_r p(1,z) &=& 0 \\ \partial_z p(r,0) &=& 0 \\ \partial_z p(r,Z_f) &=& 0 \end{array}\right. \tag{53}$$

where differences due to asymmetry are bolded.

These conditions possess the same streamwise values except for those around the centerline. This definition still requires the centerline to behave as the axis of rotation but not as the axis of symmetry.

VIII. On the Hardware Requirements of the Eigensolver

The hardware requirements are significantly higher for the biglobal approach in comparison to the one-dimensional, LNP, approach. Unlike the one-dimensional operator matrices, those presented here require conversion into product tensor form which, alone, increases the matrix size by a factor of N. According to Theofilis, [23] a minimum of 30 to 35 discretization points are required for each fluctuating variable in order to adequately describe the spatial structure of the eigenfunction. However, the spectral accuracy may not yet be refined for such few discretization points (see Fig. 8a). Reasonable convergence for the LNP approach applied to the bidirectional vortex baseflow requires no less than 400 collocation points. [22] Fortunately, the eigenvector, and therefore the hydrodynamic wave form, do not change appreciably with increased grid resolution. Even so, the required degree of computational power can exceed the limitations of current desktop computers. While the computational labor could be circumvented with a streamfunction formulation, such an approach cannot be used here, given the nature of our three-dimensional perturbations. Characteristic runtimes associated with our model are shown in Fig. 8b.

In short, the majority of the computational power may be attributed to the eigensolver. Traditional QZ and LZ algorithms compute the entire spectrum at once but are much more time consuming than Krylov subspace methods. Because of this, Arnoldi algorithms are typically substituted. [27] Arnoldi methods compute a specified number of eigenvalues located around a guess value. A common way of determining guess values is to revert to low resolution QZ or LZ algorithms. This procedure, however, poses a potential pitfall. It is shown in Fig. 8a that grid refinement is necessary to determine the minimum number of collocation points for convergence. Below this number, the spectrum shows significant dependence on N. The high frequency amplified modes shown in Fig. 8a may not be seen or properly captured through this approach.

To further exacerbate the need for a fine spectral grid, it is well known that cases with high Reynolds numbers lead to an increasingly diminished boundary layer thickness. The collocation near the wall must be such that the correct boundary layer profile is realized. Poor spacing within the boundary layer translates to an inaccurate profile and a mischaracterization of the shear stresses generated by the baseflow. Large Reynolds numbers can also cause unphysical oscillations in the interpolating polynomials because the steepness of the boundary layer profile reduces the overall smoothness of the spectral function. Table 1 provides the minimum collocation number to characterize the boundary layer with at least three points. This is done for several values of Re, V, and δ_w, using both complex-lamellar and linear Beltramian baseflow models. Note that the minimum number of required collocation points increases very quickly.

Table 1. The minimum discretization number, N, to characterize the baseflow boundary layer with at least three points

	$Re =$	1000	5000	10000	50000	100000
	$V =$	628	3142	6283	31416	62832
Complex-lamellar	$\delta_w =$	0.0230	0.0046	0.0023	0.0005	0.0002
	$N \approx$	21	44	57	150	200
Beltramian	$\delta_w =$	0.0094	0.0019	0.0009	0.0002	0.0001
	$N \approx$	40	80	100	250	350

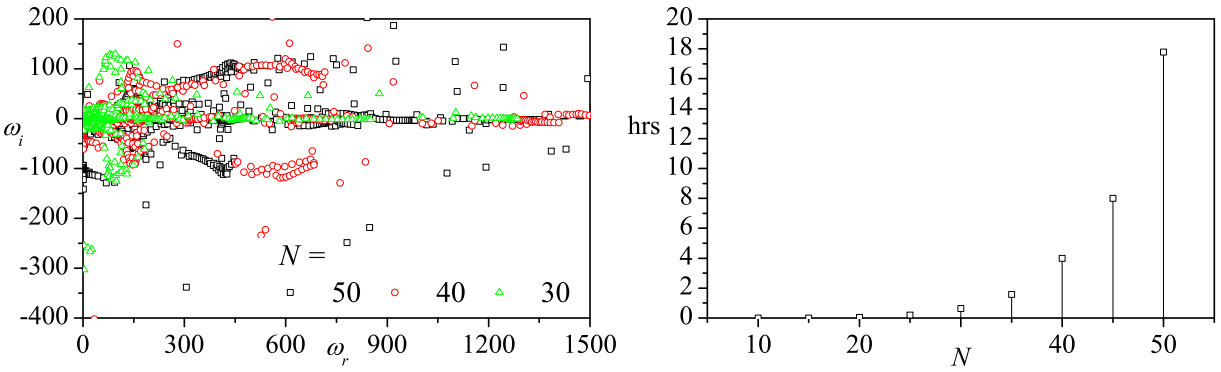

a) Grid refinement **b)** Runtime

Figure 8. The linear Beltramian spectrum and QZ algorithm runtime with increasing N on eight 2.2GHz cores, 16GB RAM, and Win7x64. Here $Re = 10,000$, $q = 1$, and $\kappa = 0.1$

.

IX. Closing Remarks

The majority of work on biglobal stability dismisses the intricate steps entailed in the problem formulation in favor of the results. Doing so minimizes the possibility for others to follow, verify, or build upon such work. The motivation for Part 1 of this series is to counter this noted deficiency by delineating a more detailed framework for the biglobal stability problem in multiple dimensions. Considerable effort will be required to translate the formulations in this article into functional code; however, it is hoped that the obscurity and mythical complexity associated with biglobal instability analysis will be substantially alleviated, if not eliminated entirely, in part by this study. The most concise discussion of the numerical application of spectral collocation methods may be found in the textbook by Trefethen. [36] Given the additional procedural detail provided here, it is hoped that the biglobal stability approach will be further extended to more complex physical settings and flow configurations. The instability of the bidirectional vortex will constitute one such example that will receive attention in this paper's Part 2 sequel. [44]

Acknowledgments

This material is based on work supported partly by the National Science Foundation through Grant No. CMMI-0928762, and partly by the University of Tennessee Space Institute, through institutional cost sharing.

References

[1]Chiaverini, M. J., Malecki, M. J., Sauer, A., and Knuth, W. H., "Vortex Combustion Chamber Development for Future Liquid Rocket Engine Applications," *38th AIAA/ASME/SAE/ASEE Joint Propulsion Conference and Exhibit*, AIAA Paper 2002-4149, Indianapolis, Indiana, July 2002.

[2]Chiaverini, M., Malecki, M., Sauer, J., Knuth, W., and Hall, C., "Testing and Evaluation of Vortex Combustion Chamber for Liquid Rocket Engines," JANNAF TP-2002-0372, Destin, Florida, April 2002.

[3]Chiaverini, M., Malecki, M., Sauer, J., Knuth, W., and Majdalani, J., "Vortex Thrust Chamber Testing and Analysis for O2-H2 Propulsion Applications," *39th AIAA/ASME/SAE/ASEE Joint Propulsion Conference and Exhibit*, AIAA Paper 2003-4473, Huntsville, Alabama, July 2003.

[4]Batterson, J. W., Maicke, B. A., and Majdalani, J., "Advancements in Theoretical Models of Confined Vortex Flowfields," JANNAF Paper TP-2007-222, Denver, Colorado, May 2007.

[5]Rankine, W., *A Manual of Applied Mechanics*, Griffin, 1877.

[6]Lamb, H., *Hydrodynamics*, Dover Publications, Cambridge, 1932.

[7]Burgers, J., "A Mathematical Model Illustrating the Theory of Turbulence," *Advances in Applied Mechanics*, Vol. 1, 1948, pp. 171–199. doi:10.1016/S0065-2156(08)70100-5.

[8]Vatistas, G., Lin, S., and Kwok, C., "Theoretical and Experimental Studies on Vortex Chamber Flows," *AIAA Journal*, Vol. 24, No. 4, April 1986, pp. 635–642. doi:10.2514/3.9319.

[9]Vatistas, G. H., "Tangential Velocity and Static Pressure Distributions in Vortex Chambers," *AIAA Journal*, Vol. 25, No. 8, August 1987, pp. 1139–1140. doi:10.2514/3.9755.

[10]Aboelkassem, Y., and Vatistas, G. H., "New Model for Compressible Vortices," *Journal of Fluids Engineering*, Vol. 129, No. 8, August 2007, pp. 1073–1079. doi:10.1115/1.2746897.

[11]Sullivan, R., "A Two-Cell Vortex Solution of the Navier-Stokes Equations," *Journal of Aerospace Sciences*, Vol. 26, June 26 1959, pp. 767–768.

[12]Bloor, M., and Ingham, D., "Theoretical Investigation of the Flow in a Conical Hydrocyclone," *Chemical Engineering Research and Design*, Vol. 51, No. 1, 1973, pp. 36–41.

[13]Bloor, M., and Ingham, D., "The Flow in Industrial Cyclones," *Journal of Fluid Mechanics*, Vol. 178, 1987, pp. 507–519. doi:10.1017/S0022112087001344.

[14]Vyas, A., Majdalani, J., and Chiaverini, M., "The Bidirectional Vortex. Part 1: An Exact Inviscid Solution," *39th AIAA/ASME/SAE/ASEE Joint Propulsion Conference and Exhibit*, AIAA Paper 2003-5052, Huntsville, Alabama, July 2003.

[15]Vyas, A., and Majdalani, J., "Exact Solution of the Bidirectional Vortex," *AIAA Journal*, Vol. 44, No. 10, October 2006, pp. 2208–2216. doi:10.2514/1.14872.

[16]Majdalani, J., and Chiaverini, M. J., "On Steady Rotational Cyclonic Flows: The Viscous Bidirectional Vortex," *Physics of Fluids*, Vol. 21, No. 10, 2009, pp. 103603–15. doi:10.1063/1.3247186.

[17]Batterson, J. W., and Majdalani, J., "Sidewall Boundary Layers of the Bidirectional Vortex," *Journal of Propulsion and Power*, Vol. 26, No. 1, October 2009, pp. 102–112. doi:10.2514/1.40442.

[18]Majdalani, J., "Exact Eulerian Solutions of the Cylindrical Bidirectional Vortex," *45th AIAA/ASME/SAE/ASEE Joint Propulsion Conference and Exhibit*, AIAA Paper 2009-5307, Denver, Colorado, August 2009.

[19]Batterson, J. W., and Majdalani, J., "On the Viscous Bidirectional Vortex. Part 1: Linear Beltramian Motion," *46th AIAA/ASME/SAE/ASEE Joint Propulsion Conference and Exhibit*, AIAA Paper 2010-6763, Nashville, Tennessee, July 2010.

[20]Batterson, J. W., and Majdalani, J., "On the Viscous Bidirectional Vortex. Part 2: Noninear Beltramian Motion," *46th AIAA/ASME/SAE/ASEE Joint Propulsion Conference and Exhibit*, AIAA Paper 2010-6764, Nashville, Tennessee, July 2010.

[21]Batterson, J. W., and Majdalani, J., "On the Viscous Bidirectional Vortex. Part 3: Multiple Mantles," *46th AIAA/ASME/SAE/ASEE Joint Propulsion Conference and Exhibit*, AIAA Paper 2010-6765, Nashville, Tennessee, July 2010.

[22]Abu-Irshaid, E., Majdalani, J., and Casalis, G., "Hydrodynamic Instability of the Bidirectional Vortex," *41st AIAA/ASME/SAE/ASEE Joint Propulsion Conference and Exhibit*, AIAA Paper 2005-4531, Tuscon, Arizona, July 2005.

[23]Theofilis, V., "Advances in Global Linear Instability Analysis of Nonparallel and Three-Dimensional Flows," *Progress in Aerospace Sciences*, Vol. 39, No. 4, May 2003, pp. 249–316. doi:10.1016/S0376-0421(02)00030-1.

[24]Theofilis, V., Duck, P. W., and Owen, J., "Viscous Linear Stability Analysis of Rectangular Duct and Cavity Flows," *Journal of Fluid Mechanics*, Vol. 505, April 2004, pp. 249–286. doi:10.1017/S002211200400850X.

[25]Pitt, R., Sherwin, S., and Theofilis, V., "BiGlobal Stability Analysis of Steady Ow in Constricted Channel Geometries," *International Journal for Numerical Methods in Fluids*, Vol. 47, April 2005, pp. 1229–1235. doi:10.1002/fld.840.

[26]Chedevergne, F., and Casalis, G., "Thrust Oscillations in Reduced Scale Solid Rocket Motors, Part II: A New Theoretical Approach," *41st AIAA/ASME/SAE/ASEE Joint Propulsion Conference and Exhibit*, AIAA Paper 2005-4000, Tucson, Arizona, July 2005.

[27]Chedevergne, F., Casalis, G., and Féraille, T., "Biglobal Linear Stability Analysis of the Flow Induced by Wall Injection," *Physics of Fluids*, Vol. 18, January 2006, pp. 014103. doi:10.1063/1.2160524.

[28]Chedevergne, F., Casalis, G., and Majdalani, J., "DNS Investigation of the Taylor-Culick Flow Stability," *43rd AIAA/ASME/SAE/ASEE Joint Propulsion Conference and Exhibit*, AIAA Paper 2007-5796, Cincinnati, Ohio, July 2007.

[29]Majdalani, J., and Flandro, G. A., "The Oscillatory Pipe Flow with Arbitrary Wall Injection," *Proceedings of the Royal Society A: Mathematical, Physical and Engineering Sciences*, Vol. 458, No. 2023, July 2002, pp. 1621–1651. doi:10.1098/rspa.2001.0930.

[30]Casalis, G., and Vuillot, F., "Motor Flow Instabilities - Part 2 Intrinsic Linear Stability of the Flow Induced by Wall Injection," Tech. rep., ONERA, Belgium, May 2002.

[31]Culick, F., "Rotational Axisymmetric Mean Flow and Damping of Acoustic Waves in a Solid Propellant Rocket," *AIAA Journal*, Vol. 4, No. 8, August 1966, pp. 1462–1464. doi:10.2514/3.3709.

[32]Majdalani, J., and Saad, T., "The Taylor-Culick Profile with Arbitrary Headwall Injection," *Physics of Fluids*, Vol. 19, No. 9, September 2007, pp. 093601–10. doi:10.1063/1.2746003.

[33]Chedevergne, F., *Instabilités Intrinsèques des Moteurs à Propergol Solide*, Ph.D. thesis, L'école Nationale Supérieure de L'aéronautique et de L'éspace, Toulouse, September 2007.

[34]Robitaillié-Montané, C., and Casalis, G., "Méthode de Collocation Spectrale Appliquée à un Problème de Stabilité donné sous Forme d'Équations aux Dérivées Partielles," Tech. Rep. RT-1/07895 DMAE, ONERA, Toulouse, March 2003.

[35]Burden, R. L., and Faires, J. D., *Numerical Analysis*, PWS-KENT Publishing Company, Boston, USA, 1989.

[36]Trefethen, L. N., *Spectral Methods in Matlab*, Society for Industrial and Applied Mathematics, Philadelphia, 2000.

[37]Arfken, G., Arfken, G., and Weber, H., *Mathematical Methods for Physicists*, Academic Press, San Diego, California, 2001.

[38]Weideman, J., and Reddy, S., "A MATLAB Differentiation Matrix Suite," *ACM Transactions on Mathematical Software*, Vol. 26, No. 4, December 2000.

[39]Quarteroni, A., Sacco, R., and Saleri, F., *Numerical Mathematics*, Springer Verlag, Berlin, 2007.

[40]Voigt, R., Gottlieb, D., and Hussaini, M., *Spectral Methods for Partial Differential Equations*, Society for Industrial and Applied Mathematics, Philadelphia, 1984.

[41]Welfert, B. D., "Generation of Pseudospectral Differentiation Matrices I," *SIAM Journal on Numerical Analysis*, Vol. 34, No. 4, August 1997, pp. 1640–1657. doi:10.1137/S0036142993295545.

[42]Elbarbary, E. M., and El-Sayed, S. M., "Higher Order Pseudospectral Differentiation Matrices," *Applied Numerical Mathematics*, Vol. 55, No. 4, December 2005, pp. 425–438. doi:10.1016/j.apnum.2004.12.001.

[43]Gottlieb, D., and Lustman, L., "The DuFort-Frankel Chebyshev Method for Parabolic Initial Boundary Value Problems," *Computers and Fluids*, Vol. 11, No. 2, 1983, pp. 107–120. doi:10.1016/0045-7930(83)90005-1.

[44]Batterson, J. W., and Majdalani, J., "Biglobal Instability of the Bidirectional Vortex. Part 2: Complex Lamellar and Beltramian Motions," *47th AIAA/ASME/SAE/ASEE Joint Propulsion Conference and Exhibit*, AIAA Paper 2011-5649, San Diego, California, July 2011.